

A Two-stage Approach for Spring Images Contour Extraction

Chao-Xuan Qin, Xiao-Hui Gu*

Abstract—Spring is a widely used mechanical equipment. The segmentation of spring images is seriously affected by intensity inhomogeneity. To solve this problem, a two-stage high-precision spring image segmentation algorithm is proposed. First, a spring measurement platform is constructed to obtain images of springs. Then a two-stage spring image contour extraction algorithm is proposed. The first stage combines the global information of the image to construct a histogram fuzzy clustering model to obtain the initial contour of the spring, then, the local information of the spring image is combined to construct a level set model to accurately extract the spring contour in the second stage. Through comparison with existing algorithms and accuracy analysis experiments, the effectiveness of the method is verified. Experimental results show that the algorithm has high accuracy, strong adaptive ability, high running speed, and can effectively suppress the problem of intensity inhomogeneity.

Index Terms—Spring, image segmentation, clustering methods, level set

I. INTRODUCTION

Spring is one of the most commonly used parts in industry. In the accelerated life test of the spring, the degradation and failure rules of the spring are obtained by detecting parameters such as the length of spring. Traditional contact measurement has large human error and reading error, image measurement is an efficient non-contact measurement technology, and image segmentation is an important part of image measurement. The aim of this paper is to propose a high precision spring image segmentation method, so the computer can automatically obtain the spring shape parameters. This technology can also be applied to online measurement, quality detection and other fields.

Image measurement technology is a key technology in modern scientific research and is widely used in many fields such as mechanical parts inspection [1, 2], medical measurement and diagnosis [3-7], physical experimental research [8, 9], agricultural science [10] and so on. Image measurement mainly includes image acquisition, image preprocessing, image segmentation, feature extraction and parameter measurement. Among them, image segmentation

has a very important impact on measurement accuracy, and related research has been a hot topic in the field of computer vision.

Intensity inhomogeneity often occurs in natural images because of imperfection in the imaging device and uneven illumination. It remains a challenge to accurately segment images with intensity inhomogeneity. To segment images with intensity inhomogeneity, Yan proposed an image segmentation method based on MRF (Markov random field) and ELM (Extreme learning machine) [11]. Mahata put forward a fuzzy algorithm integrating a Gaussian function and local contextual information within the objective function [12]. Feng utilized a linear combination of a given set of smooth orthogonal basis functions to estimate the bias field to construct a local inhomogeneous intensity clustering (LINC) model [13]. Wang proposed a local edge entropy and introduced it to active contour model to reduce the negative impact of intensity inhomogeneity [14]. Cheng utilized a region based multi-phase level set method which is based on the multi-scale local binary fitting (MLBF) and the Kullback–Leibler (KL) divergence [15]. Salhi [16] combined the neural approach with a mathematical morphology concept to segment color texture images.

The traditional image segmentation method based on global information usually failed to segment images with intensity inhomogeneity precisely. Level set algorithms [17-19] with excellent performance in terms of shape capture, received extensive attention from scholars. However, these methods are sensitive to initial contour, and need adjustment to the parameters, more iteration time is needed if the initial contour choice is not appropriate.

The fast image segmentation algorithms usually use only global information of images and cannot extract accurate edges for gray-level uneven images, and image segmentation algorithms based on local information usually require a lot of evolution and high computational cost. Therefore, this paper proposes a two-stage image segmentation algorithm. Firstly, the global information of images is used to obtain the initial edge of the target, then the edge local information is used to construct the contour evolution equation, and perform a certain evolution to obtain the final edge of the image. This method has a higher running speed under the premise of accurately extracting the target contour. The work of this paper has relatively high application value in spring and other parts of nondestructive on-line non-contact testing

The main contributions of this work are summarized as follows:

1. The clustering model is constructed by using the global information of the images to obtain the initial edge.
2. The level set model is constructed by using the local information of image edge, and the accurate edge of image is

Manuscript received September 10, 2020; revised April 26, 2021. This work was supported by the National Defense Technology Advance Research Project of China (No. 004040204).

Chao-Xuan Qin is a Ph.D. candidate of School of Mechanical Engineering, Nanjing University of Science and Technology, Nanjing 210094, China. (e-mail: 314101002287@njust.edu.cn).

Xiao-Hui Gu is a professor of School of Mechanical Engineering, Nanjing University of Science and Technology, Nanjing 210094, China. (Corresponding author, phone: 86-139-5200-3758; e-mail: gxiaohui@njust.edu.cn).

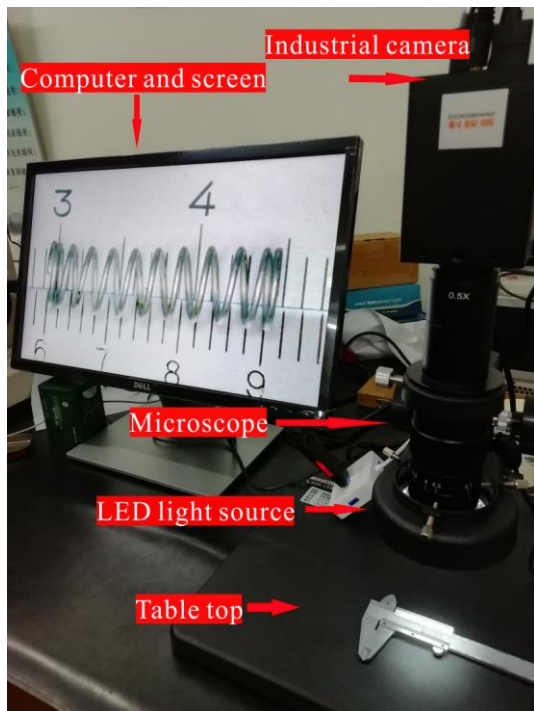


Fig. 1. Image acquisition and processing system.

obtained with less evolution.

3. The two-stage segmentation algorithm greatly improves the computing speed on the premise of ensuring the image segmentation accuracy.

4. The proposed algorithm is applied to spring image on-line measurement, and a precise result is obtained.

The remainder of the article is organized as follows: section II presents the Experimental platform and the intensity inhomogeneity phenomenon. Then, Section III describes the initial contour extraction method. Section IV describes the accurate image segmentation method. The experiment is reported in Section V and Section VI offers concluding remarks.

II. EXPERIMENTAL PLATFORM AND THE INTENSITY INHOMOGENEITY PHENOMENON

A. Experimental platform

The experimental platform is shown in Fig. 1. The spring sample is placed on the table top. The LED functions as lighting source and its brightness can be adjusted. The microscope is adjusted to the appropriate magnification, and the industrial camera is located above the microscope to obtain the image, which is then analyzed and processed in the computer. The visual range of the camera and microscope is 2.6-22mm, which means that the measurable spring size needs to be in this range. The size of sample springs tested in this paper is between 13-18mm. The camera has a resolution of 1080P and can capture high-definition images. Many cameras have the function of measurement, but require the user to operate and adjust by himself. For example, when measuring the length of springs, the user needs to manually select the boundary of the object, which is not convenient for operation and introduces human error. The algorithm proposed in this paper can automatically and accurately segment the spring image and quickly obtain the spring boundary contour, which provides great convenience for the subsequent measurement.

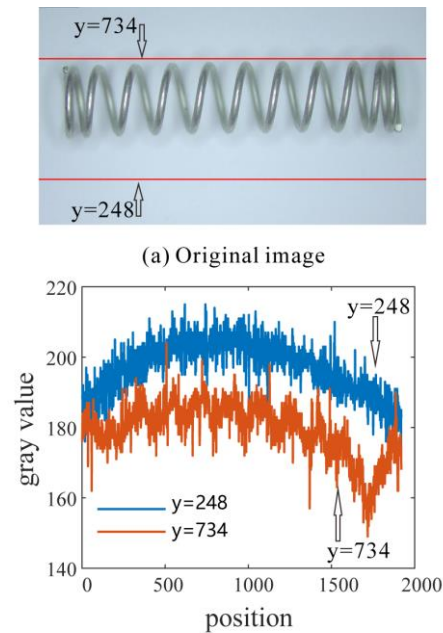


Fig. 2. Intensity inhomogeneity phenomenon in background.

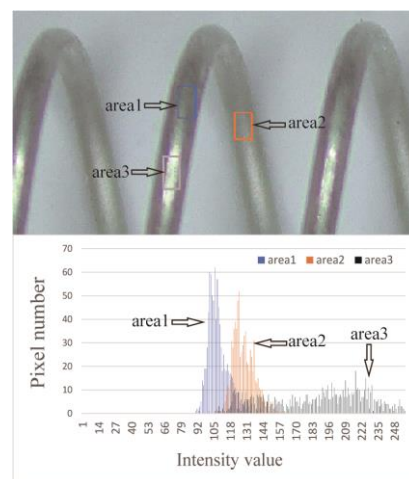


Fig. 3 Intensity inhomogeneity phenomenon in object.

B. Intensity inhomogeneity phenomenon

Science the distance between different locations of the scene and the camera is different, the light reflected to the camera sensor is different, resulting in intensity inhomogeneity, as shown in Fig. 2, where (a) is the original image and (b) is the gray value of the two horizontal lines in (a), where $y = 248$ is the pure background, and $y = 734$ contains the background and the shadow of spring under the light. The blue curve in Figure (b) shows that the gray value in the middle of the image is higher, while the gray value on both sides is lower. This is because the distance between sides and the sensor of the camera is different from that between center and camera. From the red curve we can see that the shadow leads to a lower gray value and noise exists meanwhile. The image segmentation results will be influenced by the shadow, intensity inhomogeneity and noise.

Fig. 3 shows the intensity inhomogeneity in the object area. As can be seen, the background area is the work platform, and the platform can basically be considered as a plane. The

shape of the target spring is more complicated than the background, and due to its ups and downs, the light reflected into the camera is also more complicated. Therefore, the situation of intensity inhomogeneity is more severe than the background area. So, an effective image segmentation strategy is applied to segment the background and approach the target.

III. STAGE 1 INITIAL CONTOUR EXTRACTION

In this stage, we need to quickly extract the initial edge of the spring image to prepare for the subsequent precise segmentation. From the analysis in the previous section, we can see that the spring image includes the spring target and background. Unlike some traditional algorithms such as Canny operator can be easily interfered by noise, the clustering algorithm has a certain robustness. FCM [20] (fuzzy C-means clustering) algorithm is a kind of clustering algorithm based on partition and has been widely used in the field of computer vision. The traditional segmentation algorithm of FCM image takes image pixel points as sample data, which results in large computation and slow convergence speed of the algorithm.

In this paper, the gray level information of pixels is used for clustering to map the image from the pixel space to the one-dimensional gray level histogram feature space. Thus, greatly improves the speed of calculation.

The objective function of the clustering algorithm can be expressed as:

$$\min J = \sum_{i=1}^q \sum_{k=1}^c r_i u_{ki}^m \|g_i - v_k\|^2 \quad (1)$$

where g_i is the image gray value after the Dual-Domain image filtering [21], c stands for the amount of the clusters. q is the amount of grayscale in the image and $1 < q \leq N$. u_{ki} stands for fuzzy membership of gray scale g_i to cluster k and U is the membership partition matrix.. v_k is the prototype value of the k_{th} cluster. r_i represents the number of pixels with a grayscale value of g_i and

$$\sum_{i=1}^q r_i = N \quad (2)$$

Its constraint condition of (1) is as:

$$\sum_{k=1}^c u_{ki} = 1 \quad u_{ki} \in [0, 1] \quad (3)$$

To solve the equation, construct the Lagrangian function

$$L(u_{ki}, v_k) = \sum_{i=1}^q \sum_{k=1}^c r_i u_{ki}^m \|g_i - v_k\|^2 + \lambda \left(\sum_{k=1}^c u_{ki} - 1 \right) \quad (4)$$

where λ is the Lagrange multiplier. the problem of the minimization of objective function is converted to finding the saddle point of the above Lagrange function. By taking the partial derivatives of u_{ki} and v_k (See appendix for detailed

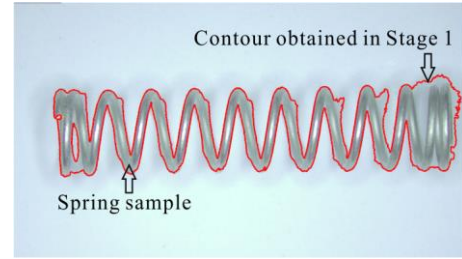


Fig. 4. Contour obtained by histogram fuzzy clustering. derivation), we finally get

$$u_{ki} = 1 / \sum_{j=1}^c (\|g_i - v_k\| / \|g_i - v_j\|)^{2/(m-1)} \quad (5)$$

$$v_k = (\sum_{i=1}^q r_i u_{ki}^m g_i) / (\sum_{i=1}^q r_i u_{ki}^m) \quad (6)$$

By calculating each u_{ki} using (5), we can get the membership partition matrix $U = [u_{ki}]^{q \times c}$. Through certain iteration, a preliminary segmentation result is formed and we can get the initial contour.

IV. STAGE 2 ACCURATE CONTOUR EXTRACTION

Through the previous clustering algorithm, we obtained a contour, as shown in Fig. 4. However, due to the existence of intensity inhomogeneity, the segmentation effect is not ideal, which requires further processing. Min [22] indicated that the intensity variation in an intensity inhomogeneity image follows a nonlinear distribution. Referring to this idea, we use the local information of the image to build a level set model. In this paper, the Taylor approximation level set method is used to further accurately segment the images.

The Taylor approximation level set method algorithm uses the nonlinear approximation method of Taylor expansion to approximate the image intensity and solve the non-convex problem of the uneven gray image. Due to the nonlinearity of the uneven gray image, it is reasonable to use the nonlinear approximation to describe the local area.

The energy functional can be expressed as:

$$E = \sum_{i=1}^2 \iint_{\Omega} k_{\sigma}(x-y) (I(x) - LIM_i(x) - b'(y) C_i)^2 H_i(\phi) dy dx + \mu \int_{\Omega} |\nabla H(\phi)| dx + \nu \int_{\Omega} (|\nabla \phi| - 1)^2 dx \quad (7)$$

where $\Omega \in R^n$ is the image domain, I denotes the input image. $y \in \Omega_x$ is the neighborhood centered at x . b' is the variation degree of intensity inhomogeneity, k_{σ} is the Gaussian kernel with standard deviation σ . μ and ν are two constant weight parameters. LIM is the local intensity defined as:

$$LIM_i(x) = \text{mean}(I(y) : y \in \Omega_x \cap \Omega_i) \quad i \in \{1, 2\} \quad (8)$$

$H_1(\phi)$ is the approximate Heaviside function and it's defined

as follows:

$$H_1(\phi) = \frac{1}{2} \left(1 + \frac{2}{\pi} \arctan \left(\frac{\phi}{\varepsilon} \right) \right) \quad (9)$$

$$H_2(\phi) = 1 - H_1(\phi) \quad (10)$$

Using standard gradient descent method to minimize the energy functional, we can get:

$$\begin{aligned} \frac{\partial E}{\partial C_1} = & \partial \iint_{\Omega} k_{\sigma}(x-y) ((I(x) - LIM_i(x))^2 + \\ & + b'^2(y) C_1^2 - 2(b'(y) C_1 (I(x) - LIM_i(x)))) \times \\ & \times H_i(\phi) dy dx / \partial C_1 \end{aligned} \quad (11)$$

$$\begin{aligned} \frac{\partial E}{\partial C_1} = & \partial \iint_{\Omega} k_{\sigma}(x-y) (2b'^2(y) C_1 - \\ & - 2(I(x) - LIM_i(x)) b'(y)) H_i(\phi) dy dx = 0 \end{aligned} \quad (12)$$

$$C_i = \frac{\iint_{\Omega} k_{\sigma}(x-y) (I(x) - LIM_i(x)) H_i(\phi) dy dx}{\iint_{\Omega} k_{\sigma}(x-y) b'(y) H_i(\phi) dy dx} \quad (13)$$

$$\begin{aligned} b'(y) = & \left(\int_{\Omega} k_{\sigma}(x-y) \sum_{i=1}^2 (I(x) - LIM_i(x)) \times \right. \\ & \left. \times C_i H_i(\phi) dx \right) / \left(\int_{\Omega} \sum_{i=1}^2 k_{\sigma}(x-y) C_i^2 H_i^2(\phi) dx \right) \end{aligned} \quad (14)$$

Similarly, by using the gradient descent method to solve the energy functional, we can obtain the contour evolution equation as:

$$\begin{aligned} \frac{\partial \phi}{\partial t} = & -\delta(\phi) \sum_{i=1}^2 \int_{\Omega} k_{\sigma}(x-y) \times \\ & \times (I(x) - LIM_i(x) - b'(y) C_i)^2 dy + \\ & + \mu \delta(\phi) \operatorname{div}(\nabla \phi / |\nabla \phi|) + \\ & + \nu (\nabla^2 \phi - \operatorname{div}(\nabla \phi / |\nabla \phi|)) \end{aligned} \quad (15)$$

where $\delta(x)$ is the derivative of $H_1(\phi)$, ∇ is the gradient operator and $\operatorname{div}(\bullet)$ is the divergence operator. The complete algorithm flow chart is shown in Fig. 5.

V. EXPERIMENT

A. Experiment of spring contour extraction effect

In order to verify the effectiveness of the method proposed in this paper, we conducted some experiments. First of all, we used this algorithm and some advanced algorithms to segment the spring image and test the effect of the algorithm by comparing the contour extraction results. After that, we segmented the vernier caliper image verified the segmentation accuracy and tested accuracy to show the application value of the algorithm proposed in this paper.

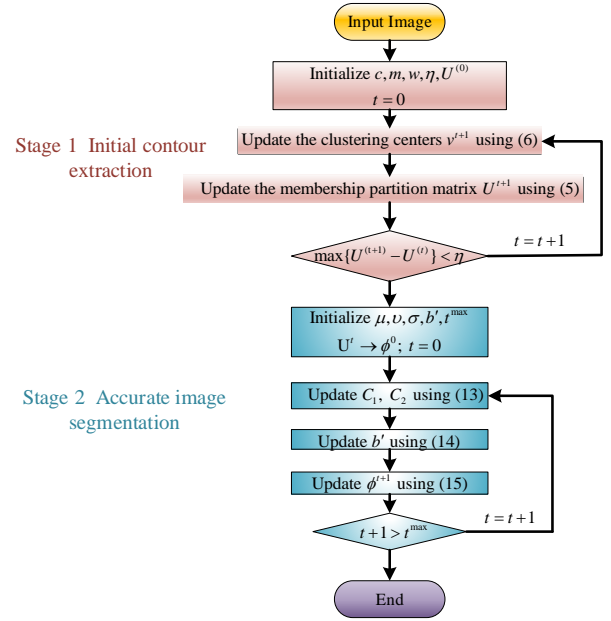


Fig. 5. Flow chart of the proposed contour extraction method.

The spring samples were used to measure the length degradation of the spring under certain conditions. The spring length and other shape parameters were tested diurnally, so the spring is photographed diurnally. Currently, there are more than 500 spring images. Here we choose 5 images under different lighting conditions as display to test the robustness of the algorithms. We segment the images into binary masks manually using Photoshop as the groundtruth.

All the experiments were implemented by MATLAB 2020a on a computer with Intel Core i5-4210U, 2.7GHz CPU and 8G RAM, Windows 10 operation system.

State-of-the-art methods were selected for comparison, namely RELSE [23], SFFCC [24] and LATE [22]. Accuracy [25], Dice [26] and Sensitivity [26] were used as the objective evaluation factors.

Accuracy measures how well the segmentation method correctly identifies or excludes a condition and it's defined as follow:

$$\text{accuracy} = \frac{TP + TN}{TP + TN + FP + FN} \quad (16)$$

where TP , TN , FP , FN denote true positive, true negative, false positive and false negative, respectively.

Sensitivity evaluates the proportion of real positives and it's defined as follows:

$$\text{sensitivity} = \frac{TP}{TP + FN} \quad (17)$$

The Sorensen-Dice similarity is another way to measure segmentation accuracy and is computed as follows:

$$\text{dice} = \frac{2TP}{2TP + FP + FN} \quad (18)$$

The experimental results are shown in Fig. 6. From top to bottom are the segmentation results of the proposed method,

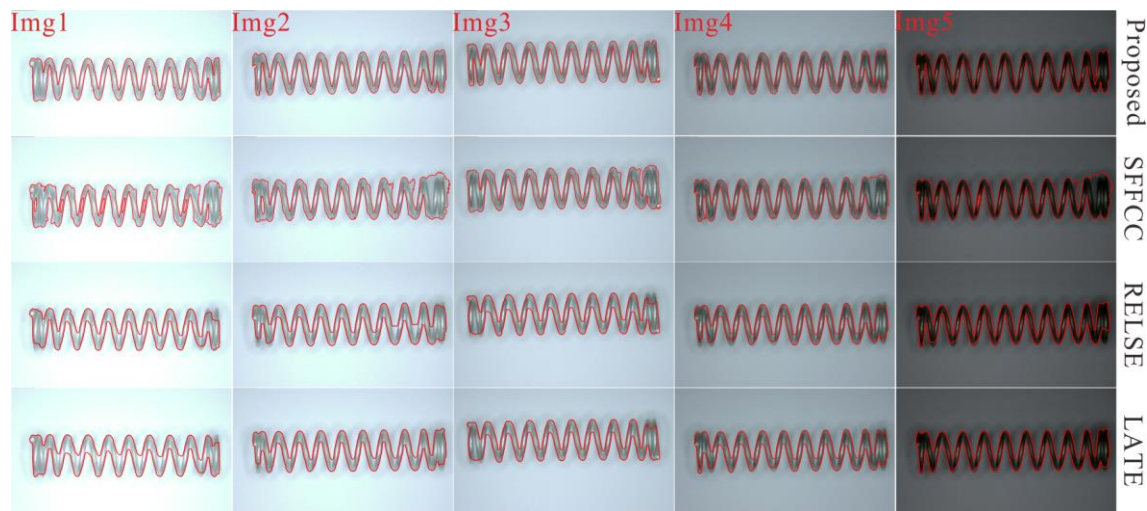


Fig.6 Spring images segmentation results using different methods.

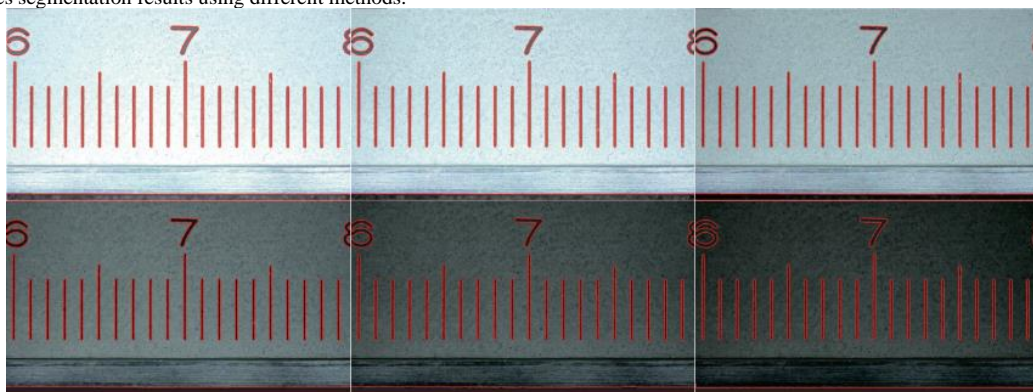


Fig.7 Vernier caliper image segmentation results.

TABLE I
THE ACCURACY RESULTS

Image	Proposed	SFFCC	RELSE	LATE
Img1	81.48	80.06	81.39	81.36
Img2	98.93	91.13	97.85	97.90
Img3	99.02	92.90	97.39	97.41
Img4	99.01	96.80	97.72	97.73
Img5	82.88	83.38	82.41	82.00

TABLE II
THE SENSITIVE RESULTS

Image	Proposed	SFFCC	RELSE	LATE
Img1	83.57	76.12	74.31	73.33
Img2	97.50	96.96	88.39	91.39
Img3	97.06	96.44	85.55	87.72
Img4	96.72	92.98	91.83	89.01
Img5	89.91	65.79	77.51	70.04

TABLE III
THE DICE RESULTS

Image	Proposed	SFFCC	RELSE	LATE
Img1	84.37	74.40	82.11	84.66
Img2	96.16	90.28	92.34	92.73
Img3	96.47	92.67	90.59	90.86
Img4	96.42	89.39	92.21	91.99
Img5	89.97	83.10	88.49	89.49

TABLE IV
THE AVERAGE RUNNING TIME

Proposed	SFFCC	RELSE	LATE
2.132s	1.935s	11.175s	10.137s

SFFCC, RELSE and LATE algorithms. SFFCC is an algorithm based on fuzzy clustering. From the figure we can see that this algorithm is not so effective at segmenting the images due to the impact of intensity inhomogeneity especially on the right side of the springs, and the shadow caused by light also has some adverse effects on the segmentation results. The result of SFFCC method has the problem of under-segmentation. RELSE and LATE are both level set methods which can obtain more accurate results and

suppress the shadow and intensity inhomogeneity to some extent. However, due to the existence of intensity inhomogeneity, the problem of over segmentation appears in some areas with serious intensity inhomogeneity, while the initial contour has a certain influence on the segmentation results, and the number of iterations is very large, resulting in a long operation time, as shown in Table IV.

The proposed algorithm combines the advantages of clustering algorithm and level set algorithm. It can be seen from the Fig. 6 that the segmentation results obtained by the algorithm in this paper are the most accurate.

It can be seen from Table I and Table II that the algorithm presented in this paper achieves the best results in terms of

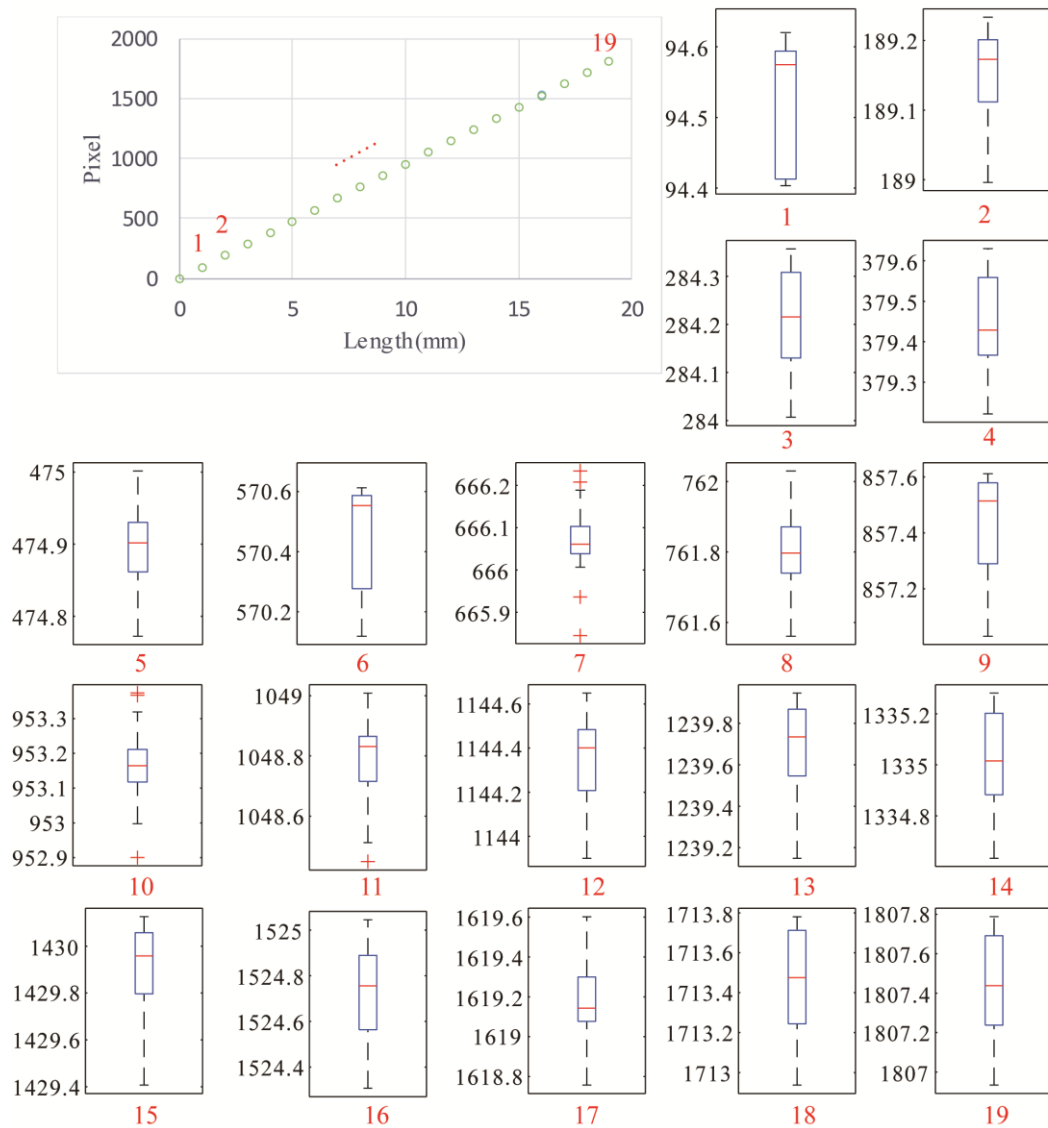


Fig.8 Image segmentation precision analysis result diagram.

accuracy and sensitive. In terms of dice index as shown in Table III, only Img1 got the second place, and the best effect was obtained in other images. Therefore, it is objectively verified that the algorithm presented in this paper has a higher segmentation accuracy than the existing algorithm.

As can be seen from Table IV, since our computational load is greater than that of clustering-based algorithms such as SFFCC, our running time is slightly higher than SFFCC. However, compared with level set based methods RELSE and LATE, the running efficiency is greatly improved.

B. Measurement precision analysis experiment

In order to verify the accuracy of the proposed algorithm applied to measurement, a vernier caliper was placed under the microscope to take pictures under different light intensity. The image was segmented by the algorithm in this paper, and then the scale was extracted for measurement. The results are shown in Fig. 7. We chose 6 photos as the display. Each image was measured six times using the proposed method. Draw scatter plot and boxplot as shown in Fig.8.

It can be seen from Fig. 7 that there are 20 scale lines in each picture. The proposed algorithm is used to extract scale

lines and calculate the central line position of the scale lines. The ordinate of the scatter plot in Fig. 8 is the central line pixel coordinate of the extracted scale lines. The first visible scale line is zero point, the abscissa is the actual position of the scale lines, and the distance between adjacent scale lines of the caliper is 1mm. It can be seen from the scatter diagram that the coordinates of pixel points at each scale are almost completely identical, which indicates that the algorithm has very high precision and linearity. In order to objectively verify the linearity of the algorithm, the scatter points were fitted linearly using MATLAB, and the fitting results are $R^2 = 1$ and $RMSE = 1.16$, which indicates that the measured results were nearly perfect linearity.

There are 19 points except zero point. The boxplot was drawn for these 19 points. For the convenience of viewing, the boxplot at each point was extracted and enlarged as shown in Fig. 8. As can be seen from these boxplots, the measurement results of each scale are very accurate, such as the measurement error of the first scale is only about 0.2 pixels. The error of all scale lines is less than 2 pixels, which verifies the accuracy of the algorithm proposed in this paper.

VI. CONCLUSION

This paper presents an efficient method for high precision contour extraction of spring images. Firstly, the spring experimental platform is built to obtain the images of the springs and we analyzed the intensity inhomogeneity phenomenon. Then the two-stage spring image precise segmentation algorithm based on histogram fuzzy clustering and Taylor approximation level set method is proposed. The algorithm combines the advantages of clustering algorithm and level set algorithm. The histogram fuzzy clustering algorithm is used to obtain an initial contour and then the Taylor approximation level set method is used to precisely segment the image to get the final result. Spring sample images were collected under different lighting conditions. Compared the proposed method with RELSE, SFFCC and LATE. Accuracy, Dice and Sensitivity were used as the objective evaluation factors. Experimental results show that the proposed algorithm can effectively suppress the problem of intensity inhomogeneity with high precision, strong adaptability and high running speed.

APPENDIX

Derivation of (5) and (6)

The Lagrange multiplier method is used to transfer the constraints to the objective function:

$$\begin{aligned} \min J = & \sum_{i=1}^q \sum_{k=1}^c r_i u_{ki}^m \|g_i - v_k\|^2 + \lambda_1 \left(\sum_{k=1}^c u_{k1} - 1 \right) + \\ & + \dots + \lambda_i \left(\sum_{k=1}^c u_{ki} - 1 \right) + \dots + \lambda_q \left(\sum_{k=1}^c u_{kq} - 1 \right) \end{aligned} \quad (19)$$

First we will solve u_{ki} by taking the partial derivative with respect to u_{ki} , Expand the first term we can get

$$\begin{aligned} \sum_{i=1}^q \sum_{k=1}^c r_i u_{ki}^m \|g_i - v_k\|^2 = & \begin{bmatrix} r_1 u_{11}^m \|g_1 - v_1\|^2 & \dots & r_1 u_{11}^m \|g_1 - v_k\|^2 & \dots & r_1 u_{11}^m \|g_1 - v_c\|^2 \\ \vdots & \vdots & \vdots & \vdots & \vdots \\ r_i u_{i1}^m \|g_i - v_1\|^2 & \dots & r_i u_{ki}^m \|g_i - v_k\|^2 & \dots & r_i u_{ci}^m \|g_i - v_c\|^2 \\ \vdots & \vdots & \vdots & \vdots & \vdots \\ r_q u_{q1}^m \|g_q - v_1\|^2 & \dots & r_q u_{qk}^m \|g_q - v_k\|^2 & \dots & r_q u_{cq}^m \|g_q - v_c\|^2 \end{bmatrix} \end{aligned} \quad (20)$$

And then we can find that u_{ki} is only contained in the term $r_i u_{ki}^m \|g_i - v_k\|^2$ in the center of the matrix, so the partial derivatives of the other terms with respect to u_{ki} are all going to be 0. And the same, in the following summation term, Only the partial derivative of $\lambda_i \left(\sum_{k=1}^c u_{kj} - 1 \right)$ with respect to u_{ki} is not 0. So we can get that:

$$\begin{aligned} \frac{\partial J}{\partial u_{ki}} = & \frac{\partial \left(r_i u_{ki}^m \|g_i - v_k\|^2 \right)}{\partial u_{ki}} + \frac{\partial \left(\lambda_i \left(\sum_{k=1}^c u_{kj} - 1 \right) \right)}{\partial u_{ki}} = \\ = & m r_i u_{ki}^{m-1} \|g_i - v_k\|^2 + \lambda_i = 0 \end{aligned} \quad (21)$$

And we can get that:

$$u_{ki}^{m-1} = - \frac{\lambda_i}{m r_i \|g_i - v_k\|^2} \quad (22)$$

Let's substitute (22) into the constraint function (3) and we can get that:

$$\sum_{i=1}^q u_{ki} = \sum_{i=1}^q u_{ki} \left(\frac{-\lambda_i}{m r_i} \right)^{\frac{1}{m-1}} \left(\frac{1}{\|g_i - v_k\|^{\frac{2}{m-1}}} \right) = 1 \quad (23)$$

And finally, we get the result:

$$u_{ki} = 1 / \sum_{j=1}^c \left(\|g_i - v_k\| / \|g_i - v_j\| \right)^{2/(m-1)} \quad (24)$$

Then, we will solve v_k by taking the partial derivative of J with respect to v_k .

$$\begin{aligned} \frac{\partial J}{\partial v_k} = & \frac{\partial \left(\sum_{i=1}^q r_i u_{ki}^m \|g_i - v_k\|^2 \right)}{\partial v_k} = \\ = & \sum_{i=1}^q r_i u_{ki}^m (2v_k - 2g_i) = 0 \end{aligned} \quad (25)$$

And we can get the result:

$$v_k = \left(\sum_{i=1}^q r_i u_{ki}^m g_i \right) / \left(\sum_{i=1}^q r_i u_{ki}^m \right) \quad (26)$$

REFERENCES

- [1] J. L. Wang, J. Zhu and S. Y. Zhang, "Based on Image Processing Technology of Video Precision Measurement System," *Applied Mechanics and Materials*, vol. 241-244, pp. 269-271, 2012.
- [2] X. WANG and X. ZHANG, "Laser and vision measurement research on parameters of miniature quartz plate-sensitive glass part," *Spectroscopy and Spectral Analysis*, vol. 34, no. 6, pp. 1450-1455, 2014.
- [3] A. Noorfizir, M. N. Rachmatullah and G. Sulong, "Hybrid Multilevel Thresholding-Otsu and Morphology Operation for Retinal Blood Vessel Segmentation.," *Engineering Letters*, vol. 28, no. 1, pp. 180-191, 2020.
- [4] L. Chen, D. Wei and J. Wang, "Research on Magnetic Resonance Imaging Segmentation Algorithm.," *Engineering Letters*, vol. 27, no. 3, pp. 559-567, 2019.
- [5] U. C. Wiesmann, S. L. F. A. Stevens and S. D. Shorvon, "Image Contrast and Hippocampal Volumetric Measurements," *Magnetic Resonance Imaging*, vol. 1, no. 16, pp. 13-17, 1998.
- [6] S. Zhou, J. Wang, S. Zhang, Y. Liang, and Y. Gong, "Active contour model based on local and global intensity information for medical image segmentation," *Neurocomputing*, vol. 186, pp. 107-118, 2016.
- [7] R. M A Ca, M. Bene V S and J. Tint V E Ra, "Segmentation of MRI Images by Adaptive Degenerate Diffusion.," *IAENG International Journal of Applied Mathematics*, vol. 45, no. 3, pp. 208-217, 2015.
- [8] A. Jahedsaravani, M. Massinaei and M. H. Marhaban, "An image segmentation algorithm for measurement of flotation froth bubble size distributions," *Measurement*, vol. 111, pp. 29-37, 2017.
- [9] B. G. Demczyk, Y. M. Wang, J. Cumings, M. Hetman, W. Han, A. Zettl, and R. O. Ritchie, "Direct mechanical measurement of the tensile strength and elastic modulus of multiwalled carbon nanotubes.," *Materials Science and Engineering: A*, vol. 334, no. 1, pp. 173-178, 2002.
- [10] G. Sanchez-Torres, A. Ceballos-Arroyo and S. Robles-Serrano, "Automatic measurement of fish weight and size by processing

- underwater hatchery images," *Engineering Letters*, vol. 26, no. 4, pp. 461–472, 2018.
- [11] Y. Song, B. He, Y. Zhao, G. Li, Q. Sha, Y. Shen, T. Yan, R. Nian, and A. Lendasse, "Segmentation of sidescan sonar imagery using markov random fields and extreme learning machine," *IEEE Journal of Oceanic Engineering*, vol. 44, no. 2, pp. 502–513, 2018.
- [12] N. Mahata, S. Kahali, S. K. Adhikari, and J. K. Sing, "Local contextual information and Gaussian function induced fuzzy clustering algorithm for brain MR image segmentation and intensity inhomogeneity estimation," *Applied Soft Computing*, vol. 68, pp. 586–596, 2018.
- [13] C. Feng, D. Zhao and M. Huang, "Image segmentation and bias correction using local inhomogeneous iNtensity clustering (LINC): a region-based level set method," *Neurocomputing*, vol. 219, pp. 107–129, 2017.
- [14] L. Wang, G. Chen, D. Shi, Y. Chang, S. Chan, J. Pu, and X. Yang, "Active contours driven by edge entropy fitting energy for image segmentation," *Signal Processing*, vol. 149, pp. 27–35, 2018.
- [15] D. Cheng, F. Tian, L. Liu, X. Liu, and Y. Jin, "Image segmentation based on multi-region multi-scale local binary fitting and Kullback–Leibler divergence," *Signal, Image and Video Processing*, vol. 12, no. 5, pp. 895–903, 2018.
- [16] K. Salhi, E. M. Jaara, M. T. Alaoui, and Y. T. Alaoui, "Color-Texture Image Clustering Based on Neuro-morphological Approach," *IAENG International Journal of Computer Science*, vol. 46, no. 1, pp. 134–140, 2019.
- [17] C. Li, C. Xu, C. Gui, and M. D. Fox, "Level set evolution without re-initialization: a new variational formulation," in *2005 IEEE computer society conference on computer vision and pattern recognition (CVPR'05)*, San Diego, CA, USA, June 2005, pp. 430–436.
- [18] Z. Zhang, C. Duan, T. Lin, S. Zhou, Y. Wang, and X. Gao, "GVFOM: a novel external force for active contour based image segmentation," *Information Sciences*, vol. 506, pp. 1–18, 2020.
- [19] L. Wang, L. Zhang, X. Yang, P. Yi, and H. Chen, "Level set based segmentation using local fitted images and inhomogeneity entropy," *Signal Processing*, vol. 167, p. 107297, 2020.
- [20] J. C. Bezdek, R. Ehrlich and W. Full, "FCM: The fuzzy c-means clustering algorithm," *Computers & Geosciences*, vol. 10, no. 2, pp. 191–203, 1984.
- [21] C. Qin and X. Gu, "Improved PSO Algorithm Based on Exponential Center Symmetric Inertia Weight Function and Its Application in Infrared Image Enhancement," *Symmetry*, vol. 12, no. 2, p. 248, 2020.
- [22] H. Min, W. Jia, Y. Zhao, W. Zuo, H. Ling, and Y. Luo, "LATE: A level-set method based on local approximation of Taylor expansion for segmenting intensity inhomogeneous images," *IEEE Transactions on Image Processing*, vol. 27, no. 10, pp. 5016–5031, 2018.
- [23] W. Zhang, X. Wang, W. You, J. Chen, P. Dai, and P. Zhang, "RESLS: Region and Edge Synergetic Level Set Framework for Image Segmentation," *IEEE Trans Image Process*, vol. 29, pp. 57–71, 2020.
- [24] T. Lei, X. Jia, Y. Zhang, S. Liu, H. Meng, and A. K. Nandi, "Superpixel-Based Fast Fuzzy C-Means Clustering for Color Image Segmentation," *IEEE Transactions on Fuzzy Systems*, vol. 27, no. 9, pp. 1753–1766, 2019.
- [25] D. N. Thanh, V. S. Prasath, N. N. Hien, and Others, "Melanoma skin cancer detection method based on adaptive principal curvature, colour normalisation and feature extraction with the ABCD Rule," *Journal of Digital Imaging*, vol. 33, no. 3, pp. 574–585, 2019.
- [26] A. A. Taha and A. Hanbury, "Metrics for evaluating 3D medical image segmentation: analysis, selection, and tool," *BMC medical imaging*, vol. 15, no. 1, p. 29, 2015.

Chao-Xuan Qin received the B.Sc. degree in School of Mechanical Engineering, Nanjing University of Science and Technology, China in 2014. He is currently a Ph.D. degree candidate in Armament Science and Technology at School of Mechanical Engineering, Nanjing University of Science and Technology, China. His main research interests include computer vision, signal processing and target identification.

Xiao-Hui Gu received the Ph.D. degrees in Armament Science and Technology from School of Mechanical Engineering, Nanjing University of Science and Technology, China in 2002. He is currently a professor at School of Mechanical Engineering, Nanjing University of Science and Technology, China. His main research interests include computer vision, artificial intelligent and reliability engineering.